Surface & Coatings Technology 206 (2011) 646–653

Contents lists available at ScienceDirect

Surface & Coatings Technology

journal homepage: www.elsevier.com/locate/surfcoat

CF_x thin solid films deposited by high power impulse magnetron sputtering: Synthesis and characterization

S. Schmidt [a,*], G. Greczynski [a], C. Goyenola [a], G.K. Gueorguiev [a], Zs. Czigány [b], J. Jensen [a], I.G. Ivanov [c], L. Hultman [a]

[a] Thin Film Physics Div., Department of Physics (IFM), Linköping University, SE-581 83, Sweden
[b] Research Institute for Technical Physics and Materials Science, Hungarian Academy of Sciences, P.O. Box 49, H-1525 Budapest, Hungary
[c] Semiconductor Materials Div., Department of Physics (IFM), Linköping University, SE-581 83, Sweden

ARTICLE INFO

Available online 3 July 2011

Keywords:
Fluorine containing carbon thin films
HiPIMS
CF_x
First principle calculations
XPS
TEM

ABSTRACT

Fluorine containing amorphous carbon films (CF_x, $0.16 \leq x \leq 0.35$) have been synthesized by reactive high power impulse magnetron sputtering (HiPIMS) in an Ar/CF_4 atmosphere. The fluorine content of the films was controlled by varying the CF_4 partial pressure from 0 mPa to 110 mPa at a constant deposition pressure of 400 mPa and a substrate temperature of 110 °C. The films were characterized regarding their composition, chemical bonding and microstructure as well as mechanical properties by applying elastic recoil detection analysis, X-ray photoelectron spectroscopy, Raman spectroscopy, transmission electron microscopy, and nanoindentation. First-principles calculations were carried out to predict and explain F-containing carbon thin film synthesis and properties. By geometry optimizations and cohesive energy calculations the relative stability of precursor species including C_2, F_2 and radicals, resulting from dissociation of CF_4, were established. Furthermore, structural defects, arising from the incorporation of F atoms in a graphene-like network, were evaluated. All as-deposited CF_x films are amorphous. Results from X-ray photoelectron spectroscopy and Raman spectroscopy indicate a graphitic nature of CF_x films with $x \leq 0.23$ and a polymeric structure for films with $x \geq 0.26$. Nanoindentation reveals hardnesses between ~1 GPa and ~16 GPa and an elastic recovery of up to 98%.

1. Introduction

Carbon-based thin films offer a wealth of properties for the design of, e.g. tribological and wear resistant coatings. This applies to diamond-like carbon of varying sp^2-to-sp^3 bonding ratio for the tuning of hardness and friction as well as to the fullerene-like (FL) modification in carbon nitride (CN_x) [1] and phosphorous carbide (CP_x) [2], yielding in a remarkable combination of resiliency and hardness. Fullerene-like carbon thin films are created by the substitution of nitrogen or phosphorous for carbon which promotes heavily bent and cross-linked carbon sheets because of geometric defects, such as pentagons and sp^3-hybridization between the carbon atoms, within the sp^2-coordinated sheets. While the deformation energy is mainly stored elastically due to bending of the sheets, the high strength originates from the cross linking of the sheets preventing them from slipping [3]. In order to further explore this area of carbon-based thin films produced via reactive high power impulse magnetron sputtering (HiPIMS), fluorine was chosen as an alloying element. Fluorine has two more valence electrons compared to nitrogen and phosphorous, and its electronegativity is much higher. Different to nitrogen and phosphorous, fluorine possesses no similar valence structure to carbon. Thus, the effect of the structural incorporation of fluorine into the carbon matrix should be substantial.

So far, reports on the synthesis of fluorinated amorphous carbon films have centered mainly on different chemical vapor deposition (CVD) techniques [4] like plasma enhanced CVD (PECVD) or radio frequency PECVD (r.f.-PECVD) [5,6]. CF_x thin films were found to exhibit highly interesting electrical and optical properties. Endo et al. [7] reported dielectric constants below 2.6 depending on the F concentration for films deposited via PECVD and Agraharam et al. [5] reported even lower dielectric constants for tuned deposition parameters. A low refractive index ranging between 3 and 1.5 was found by Jung et al. [6] for CF_x films which were produced in an r.f. sputter setup. It is generally agreed that the fluorine content determines whether the film is of diamond- or polymer-like nature which, in turn, influences the film properties to a great extent. For example, F-rich films were found to possess a soft polymeric structure and low stability in presence of X-rays due to the high amount of C – F bonds [8], [9], [10], [11]. CF_x films with $0 < x < 0.25$, on the other hand, present a combination of low friction, wear resistance and moderate hardness as well as biocompatibility [8]. Hardness values, highly depending on the F concentration, between 15 GPa and 0.5 GPa were reported for example by Bendavid et al., Bottani et al. and Jacobsohn et al. [12],

* Corresponding author. Tel.: +46 13 288 974; fax: +46 13 137 568.
E-mail address: sussc@ifm.liu.se (S. Schmidt).

0257-8972/$ – see front matter © 2011 Elsevier B.V. All rights reserved.
doi:10.1016/j.surfcoat.2011.06.055

[13], [14]. This combination of film properties opens even a wider application range for CF_x coatings.

HiPIMS offers the advantage of an increased ionized flux of the target material, due to a high temporal electron density in the plasma. Furthermore, the ion flux and the ion-to-neutral flux may be controlled to a certain extent by applied bias voltage and pulse energy settings, respectively. The increased ion flux results in improved film densities, which was was recently reported by Samuelsson et al. for commonly sputtered metals [15]. Whereas, the film growth mechanism might be traced back to the subplantation model as described by Lifshitz et al. [16]. Furthermore, Weichart et al. reported an improved step coverage for Cu and Ti using HiPIMS [17]. Ionization potentials of carbon ($I_C = 11.2$ eV) and commonly sputtered metals such as titanium or copper ($I_{Ti} = 6.8$ eV, $I_{Cu} = 7.7$ eV) differ to great extent, which is mirrored in the ionized flux fraction of 4.2% for C [18] and 70% for Cu [19]. This implies that the above mentioned advantages using HiPIMS might be less pronounced in case of carbon. However, extensive studies on the synthesis and the properties of carbon-based thin films produced via HiPIMS are still lacking. At the same time, HiPIMS was reported to improve the adhesion of DLC coatings by applying an HiPIMS-based substrate pre-treatment [20].

Reactive HiPIMS has not yet been applied for the synthesis of CF_x films. Due to the elevated amount of ionized plasma species, HiPIMS might open new possibilities for the incorporation of fluorine into the carbon matrix and, hence, tailoring of film properties. Other motivations to synthesize CF_x thin films via HiPIMS lie in (i) the flexibility of the sputter process; parameters such as pulse energies, pulse frequencies (between 100 Hz and 1000 Hz), pulse lengths (between 50 μs and 200 μs), and gas flow ratios can be easily varied, not only in order to tailor film properties, but also to establish stable, reproducible processes and (ii) the usage of facilities at moderate cost; namely, the carbon target, tetrafluoromethane, and argon.

Due to the inherent high reactivity of fluorine, films of lower alloy substance, similar to FL-CN_x and FL-CP_x ($0<x<0.3$), are difficult to produce via reactive magnetron sputtering. Therefore, the control of the F/C ratio is a key issue in CF_x films for wear-resistant coatings and enhanced optical property applications.

In this paper, we studied the structural formation of CF_x ($0.16 \leq x \leq 0.35$) thin films and defects induced by fluorine in the carbon network. Theoretical calculations and the synthesis via reactive HiPIMS of CF_x films were carried out in order to assess a process window and subsequently to explore the properties of such films.

2. Computational and experimental details

The synthetic growth concept (SGC) for modeling of the film formation during vapor phase deposition [21] was applied to model the most abundant precursor species and structure-defining defects for CF_x. The framework adopted for the calculations is density functional theory (DFT) within its generalized gradient approximation (GGA) as implemented in the Gaussian 03 code [22]. The Perdew–Wang exchange-correlation function (PW91) [23], known to provide an accurate description of the structural and electronic properties of carbon-based thin films and similar covalent systems [24], was used. The stability of neutral and anionic species of CF_n ($1 \leq n \leq 4$) as well as F_2 and C_2 was investigated. Aspects of structure-defining defects in CF_x were addressed considering finite graphene-like model systems where carbon atoms are substituted by fluorine atoms. Simulations involved both geometry optimizations[1] and cohesive energy calculations. The cohesive energy per atom $E_{coh/at}$ of a species (Eq. 1) is defined as the energy required for splitting the considered system into isolated atomic species divided by the number of carbon (N_C), and fluorine atoms (N_F):

$$E_{coh/at} = \frac{E_{total} - \sum_i E_{i,total}^{isolated}}{N_C + N_F}, \quad (1)$$

where E_{total} is the energy of the relaxed species and i represents the index of summation over its constituent atoms.

CF_x thin films were deposited in an industrial coating system CC800/9 (CemeCon AG, Germany) which allows driving two out of four cathodes in HiPIMS mode and offers the possibility to operate the substrate table simultaneously in HiPIMS mode. The system consists of a vacuum chamber, where two turbo pumps (THP2101) with a nominal volume of 2100 l/s are attached. More detailed information as for the vacuum system can be found in [25]. During the deposition the turbo pumps were operated at 66% of the maximum speed. The substrates were facing the rectangular, pure graphite target (440 cm^2) at a distance of 55 mm. Reactive sputtering in an Ar/CF_4 atmosphere was performed at a constant deposition pressure of 400 mPa and the CF_4 partial pressure (p_{CF_4}) was varied between 15 mPa and 110 mPa. The cathode was operated in a power-regulated mode with a frequency of 300 Hz, an average power of 1400 W, and the pulse width kept constant at 200 μs. A temperature of 110 °C was applied to conventional B-doped Si(001)-substrates. The substrate table was operated in voltage-regulated mode. A pulsed bias voltage of −60 V was set for all processes, just exceeding the floating potential ranging between −50 V and −58 V. Current–voltage wave forms were recorded with a Tektronix DPO4054 500 MHz bandwidth digital oscilloscope.

The film thickness and thus the deposition rates were determined using cross-sectional secondary electron microcopy (SEM, LEO 1550 Gemini, Zeiss, Germany). Composition and areal atomic density of the CF_x films were evaluated using time-of-flight elastic recoil detection analysis (ToF-ERDA) applying an 40 MeV $^{127}I^{9+}$ ion beam at 22.5° incidence angle relative to the surface [26], [27]. Data were stored event by event in list mode and analyzed off-line. Data taken during the first minutes (yielding sufficient statistics) were used. Using the combination of cross-sectional SEM and ToF-ERDA the film density could be determined with an experimental error of ±10%.

X-ray photoelectron spectroscopy (XPS) was performed on a Quantum 2000 spectrometer from PHI Physical Electronics, Inc, USA using a monochromatic Al(K_α) X-ray beam ($h\nu = 1486.6$ eV) and a chamber pressure of less than 1.4E-6 Pa. XPS data of the C1s, F1s, and O1s regions were collected from samples without previous sputter cleaning, as the C–F bonding structure was reported to be easily affected [11]. Automatic charge compensation was applied, due to the fact that our films showed electrical resistivities higher than 14 Ω cm. Obtained spectra were fitted using Voigt peak shape, with the Lorentzian contribution not exceeding 20%. The full width at half maximum (FWHM) was restricted to 2 eV for all peaks. A Shirley-type background was used and all spectra were referenced to the C–C (C–CH) bond at 285 eV.

Raman spectra were obtained at room temperature in near-backscattering geometry using a high-resolution single monochromator (Jobin-Yvon HR460) equipped with a charge-coupled device (CCD) camera and a notch filter. The 363.8 nm line of an Ar^+-ion laser was applied for excitation, resulting in ~30 mW of laser power at the sample and a spot diameter of ~100 μm.

For plan-view transmission electron microscopy (TEM), CF_x films of less than 50 nm in thickness were deposited on cleaved NaCl substrates. These films were floated off in water, rinsed twice and collected on a TEM Cu grid. Cross sectional TEM was carried out on cleaved samples. Plan-view samples were examined in a Tecnai G2 TF

[1] The term "geometry optimizations" denominates the computational process carried out in order to achieve the equilibrium structure (corresponding to potential energy minimum) of a given system by iterative atomic rearrangements followed by an evaluation of inter atomic forces. When inter-atomic forces and correspondingly the potential energy of the model system meet certain pre-defined criteria (minimum values), the equilibrium structure is obtained and the geometry optimization process is concluded.

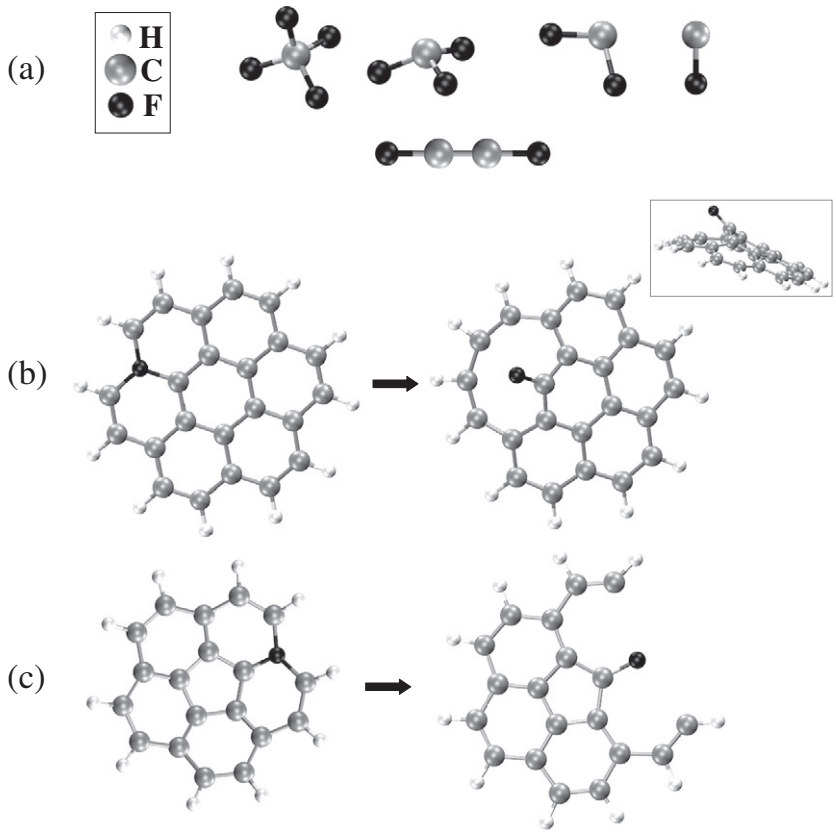

Fig. 1. a) Relaxed conformations of radicals CF, CF_2, CF_3, and C_2F_2, as well as that of the CF_4 molecule; b) A F-containing coronene model system evolving to an 8-member ring conformation after a relaxation and c) F-containing corannulene system undergoing a typical branching, which is a defect representing a typical structural pattern in CF_x due to the disruption of the C network by an incorporated F atom. Inset in b) illustrates the C – F bond rotation and the curvature of the model system.

20 UT TEM (FEI, The Netherlands). Selected area electron diffraction (SAED) patterns were exposed on imaging plates in a Philips CM20 TEM (operated at 200 kV) and high-resolution TEM (HRTEM) investigations were made in a JEOL3010 TEM operated at 300 kV from cross-sectional samples. The diffraction patterns were processed with process diffraction software [28].

The mechanical properties of the deposited films were tested in a setup combining an atomic force microscope (Nanoscope IIIa, Digital instruments) and a nanoindenter (Performech, Hyistron Inc.). Indentation tests were performed using a three-sided Berkovich tip, which was calibrated with fused silica. Every film was tested in the load-controlled mode; applying at first ten indents of decreasing loads between 1500 μN and 100 μN and next at least twenty indents utilizing a maximum load of 100 μN. From those tests, data for evaluation were considered that met the requirement to exhibit an indentation depth of 10% or less of the film thickness. Data was fitted using the Triboscope (Hyistron Inc.) software in the range of 95% to 20% of the unload curve.

3. Results and discussion

3.1. First-principles study on the formation of fluorine-containing carbon compounds

Relaxed conformations of possible precursors present in the CF_x growth environment, specifically the radicals CF, CF_2, CF_3, and C_2F_2 as well as the CF_4 molecule, the C_2, and the F_2, are displayed in Fig. 1a). Bond lengths, bond angles and the cohesive energy per atom ($E_{coh/at}$) for neutrals as well as corresponding anions are summarized in Table 1. $E_{coh/at}$, as defined by Eq. (1), permits realistic energy comparisons between precursors and model systems containing different numbers of carbon and fluorine atoms. Considering the stability

Table 1
Structural features of CF_x precursors. Some species, e.g., F_2 and CF_4 do not exist as stable anions, hence no values are provided. Since C_2F_2 species is a secondary, i.e., a recombination species, its characteristics are shown in parentheses (see main text for details).

Precursor	Neutral species			Anion species		
	Bond length, Å	Bond angle, deg.	$E_{coh/at}$, eV	Bond length, Å	Bond angle, deg	$E_{coh/at}$, eV
C_2	1.41	–	4.39	1.33	–	6.31
F_2	1.42	–	1.29	–	–	–
CF	1.30	–	3.81	1.49	–	3.89
CF_2	1.33	103.9	4.77	1.48	99.7	4.45
CF_3	1.34	111.1	4.67	1.34	–	4.77
CF_4	1.34	109.5	4.95	–	–	–
C_2F_2	C–C 1.20 C–F 1.30	(180.0)	(5.58)	–	–	–

criterion, expressed by $E_{coh/at}$, the following species appear relevant to CF_x film formation:

i Chemically reactive CF_n radicals resulting from dissociation of the CF_4 molecules (i.e. CF/CF^-, CF_2/CF_2^-, CF_3/CF_3^- cf. Table 1 for $E_{coh/at}$). Their reactivity decrease and, as judged by $E_{coh/at}$, their abundance increase according to the sequence $CF/CF_2/CF_3$. Although, CF_3 is most abundant its impact on the film formation decreases due to its lower reactivity [29] and the fact that it has a single dangling bond. CF_3 may contribute to consume dangling bonds on the film surface whereas CF_2 which is subsequent in abundance, but has a higher reactivity, exerts more significance for the bonding character of CF_x films.
ii The C_2 dimer in its neutral and ionized form is a usual building block for magnetron sputtered carbon-based thin films like FL-CN_x, FL-CP_x, and FL-CS_x [30], [31].
iii The CF_4 molecule is considered to play a less pronounced role for the CF_x film formation due to its comparatively high $E_{coh/at}$ (4.95 eV/at).
iv The F_2 as a highly reactive gas should exert a considerable impact on the film formation. However, its presence in the deposition chamber may result only from secondary recombination reactions.
v Difluoroethyne C_2F_2 resulting, e.g., from recombination of two CF species. It may play a role as desorption agent during growth and is therefore related to the removal of F from the substrate.

Our theoretical results on film-forming precursors agree with studies of isolated species for C_2 [30], C_2F_2 [32] and CF_n radicals [29]. Precursors of significance during magnetron sputtering deposition of CF_x films are CF and CF_2 radicals, the C_2 dimers, and to a lower extent free C and F atoms as well as CF_3.

The following structure-defining defects induced by substitution of a carbon atom by a fluorine atom in the graphene-like network were obtained for the CF_x compound (model systems before optimization shown in left panels in Fig. 1b) and c), respectively):

i Large N-member (N = 8–12) rings, e.g. an eight-member ring (as shown in the right panel of Fig. 1b) with one of its carbon atoms bonded to a fluorine atom, thus, creating a reactive site in the network. As the inset in Fig. 1b illustrates, a C – F bond rotation is present indicating a possible cross-link between adjacent graphene-like sheets. The gain in $E_{coh/at}$ resulting from the opening of the large 8-member ring shown in the right panel of Fig. 1 b) is $\Delta E_{coh/at} = 0.405$ eV/at;
ii A defect by branching of the model system resulting in two symmetric arms of carbon chains. Again, a C – F bond rotation is observed (right panel of Fig. 1c). The branching introduces an increased reactivity and a less ordered network. $\Delta E_{coh/at}$ in this case is 0.383 eV/at.

Large N-member rings and branching can arise from different initial structural configurations including any combination of defects (pentagons, double pentagons, Stone–Wales defects, and even tetragons) in the sense of SGC [30], [31], thus, appearing as prevailing structural features in CF_x. Both structure-defining defects contribute to intermixing of sp^3 and sp hybridization with the initial sp^2 hybridization of a pure graphene-like network. This leads to an amorphous system, especially if the F content in the film considerably exceeds 15 at.%. However, a strongly interlinked fullerene-like structure, similar to that of FL-CP_x [31], cannot be excluded at lower fluorine contents as indicated by the structural pattern of large-ring defects.

3.2. Synthesis of CF_x thin films

A set of current–voltage wave forms as a function of CF_4 partial pressure is shown in Fig. 2. The voltage is not constant throughout the pulse, but drops from the peak value at the beginning of the pulse when the charge is drawn from the capacitor bank and the plasma is ignited. Simultaneously, the target current increases to reach the peak value at the time instant that corresponds to the fastest drop in target voltage. Up to a CF_4 partial pressure of 42 mPa the peak target current is comparable for all applied processes, but a steady increase is observed at higher partial pressures (cf. inset Fig. 2). This indicates, that the amount of charged, sputtered species is increased, which may be attributed to an increased number of easily ionized species in the targets vicinity and an increase in the secondary electron emission yield γ_{SE} resulting from the changed sputter gas as well as the reactions taking place at the surface of the target [33], [34].

First and foremost, the changed surface chemistry at elevated CF_4 partial pressures is the primary reason for a different secondary electron emission yield. When the CF_4 partial pressure exceeds 42 mPa the target reacts with impinging ions as the impingement rate of the ionized species onto the target is higher than the removal rate. Thus, the target current rises due to an increased secondary electron emission from the altered surface.

At elevated CF_4 partial pressures the secondary electron yield is also affected by the different ionization potentials of Ar and CF_4 ($I_{Ar} = 15.76$ eV, $I_{CF4} = 16.91$ eV [35]). For ion energies below 1 keV, which is the case for the here applied processes, γ_{SE} is entirely depending on the target material and the sputter gas. The generation of the secondary electrons takes place via so called potential emission and γ_{SE} can be estimated applying Eq. (2);

$$\gamma_{SE} = 0.032(0.078\ I - 2\phi), \tag{2}$$

where I is the ionization potential of the impinging ions (the sputter gas) on the target surface and ϕ is the work function of the target material. An approximation of γ_{SE}, only by the change in sputter gas using Eq. (2) [34], yielded in an increase of ~34% between processes in pure CF_4 and pure Ar atmospheres, assuming the sputter process was carried out with an untainted graphite target surface. An altered secondary electron yield will furthermore affect the ion target current density, which in turn can be calculated with Eq. (3) [22];

$$j_i = \frac{j_{Tav}}{1 + \gamma_{SE}}, \tag{3}$$

where j_{Tav} is the average target current. Using Eqs. (2) and (3), the effect of a different sputter gas on the ion target current density could be estimated to yield an increase by ~50%.

Moreover, since the ionization potentials from fractured CF_4 species are considerably lower ($I_{CF} = 9.11$ eV, $I_{CF2} = 11.44$ eV and $I_{CF3} = 8.9$ eV [35]) than for CF_4 it is reasonable to assume an increased importance of those ionized radicals contributing to the plasma chemistry. Therefore, we expect that a cascade is progressing as p_{CF_4} rises above 42 mPa influencing the peak target current as shown in the inset of Fig. 2.

Worth mentioning are the comparatively low peak target currents between 82 A and 127 A observed for the described process, whereas Greczynski et al. reported values up to 650 A for a Cr/Ar discharge using a similar experimental setup [36]. The low peak target current for the carbon discharge might describe the lower end of a HiPIMS process and is attributed to the high ionization potentials of carbon, CF_4 and Ar causing a low secondary electron yield.

The deposition rate, however, first increases steeply as the CF_4 partial pressure increases followed by a decrease for $p_{CF_4} > 42$ mPa (Fig. 3). The simultaneous decrease in deposition rate and increase in target current above $p_{CF_4} = 42$ mPa indicate a less effective sputter process. In consequence of the lowered sputter yield, the deposition rate decreases as it was anticipated for the case where carbon is reactively sputtered in an Ar/N atmosphere [33]. This can be attributed to a combination of a changed target surface chemistry and an increased number of fractured, light CF_4 species that do not equal the momentum transfer of Ar. Another factor influencing the deposition rate, not coupled to the target current, is the higher probability to

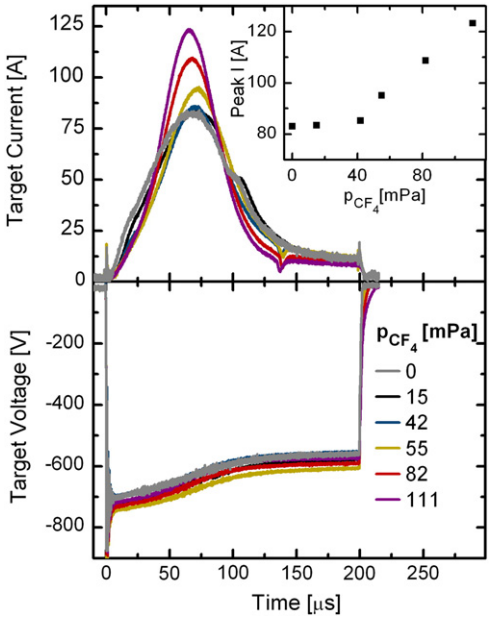

Fig. 2. Recorded target current and voltage waveforms of the deposition processes as a function of CF_4 partial pressure. The inset illustrates the increasing peak target current (I) with increasing CF_4 partial pressure.

form C_2F_2 species, when increasing p_{CF_4}. According to our theoretical studies, C_2F_2 species play a role as desorption agent during growth as well as in the removal of F atoms from the substrate surface.

ERDA results for the film composition are presented in Fig. 3. As expected, the fluorine content of the films increases as p_{CF_4} increases. The fluorine content shows a peak value of 35 at% at p_{CF_4} ~80 mPa. A further increase in CF_4 partial pressure to ~110 mPa, however, yields merely in a reduction to a value of 30.6 at% of fluorine within the films. According to our theoretical results this reduction of fluorine is attributed to the higher amount of fluorine etchants, in particular C_2F_2 species. On the other hand, films with less than 16 at% fluorine could not be obtained from the applied reactive HiPIMS process with CF_4. ERDA furthermore revealed oxygen contents of 1 at% or below and hydrogen contents below 3 at% in all examined samples. The density of the synthesized CF_x films ranged between 1.4 g/cm^3 ± 0.1 g/cm^3 and 1.6 g/cm^3 ± 0.2 g/cm^3, which is lower than that of graphite, and attributed to the incorporation of fluorine [14], [37].

3.3. Effects of fluorine on the chemical bonding and microstructure of CF_x thin films

Fig. 4 exemplifies XPS spectra of the C1s region for a sample containing 23 at% fluorine. We chose to deconvolute the C1s spectra

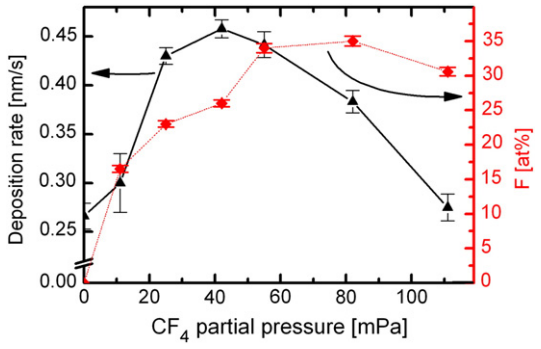

Fig. 3. Deposition rate (DR) and the fluorine content (F) obtained from ERDA measurements of CF_x thin films as a function of the CF_4 partial pressure.

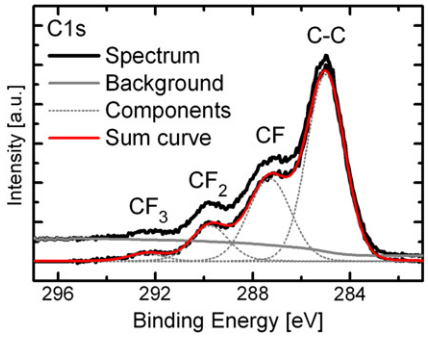

Fig. 4. XPS C1s spectrum of a $CF_{0.23}$ film with indicated peak deconvolution.

into the CF_n (n = 1–4) bonding regions due to (i) the variety of possible bonding types between carbon and fluorine, (ii) the stochastic nature of the bond-formation process (the lack of repeating unit cell like in the case of polymers) and (iii) presence of nearest-neighbor effects. For example, the region in Fig. 4 assigned to CF includes contributions from carbon atoms bonded to fluorine and contributions from those carbon atoms that are bonded to CHF (secondary chemical shifts). This approach results in broader component peaks with a FWHM not higher than 2 eV. The following bonding types within the C1s spectra are identified for films with $0.16 \le x \le 0.23$: C–C/CH–C at 285 eV, CF/C–CF at 287 eV, CF_2/C–CF_2 at 289.8 eV and C–CF_3/CF_3 at 292.4 eV. These peak assignments are in agreement with the results reported in references [38], [39], [40], [41]. Films with higher fluorine contents ($0.26 \le x \le 0.35$) show comparable binding energies for CF/C–CF at 287.0 eV ± 0.4 eV. The CF_2/C–CF_2 contributions appear shifted towards lower binding energy (289.0 eV ± 0.3 eV) and so does the C–CF_3/CF_3 component (291.2 eV ± 0.4 eV). This can be attributed to an increased amount of C affected by the neighboring carbon atom bonded to fluorine. Additionally, a contribution can be distinguished at the binding energy of 293.6 ± 0.4 eV. The relatively high binding energy of that fifth contribution and the applied film deposition method suggest an incorporation of CF_4. Based on first principle calculations for the sequence of events during thin film formation we assume that not all of CF_4 gets readily decomposed in the plasma during deposition at $p_{CF_4} > 42$ mPa. With the first ionization potential of 16.91 eV [35] a significant fraction of non-decomposed CF_4 molecules may thus be effectively ionized during energetic HiPIMS discharge, get attracted by substrate potential and become incorporated into the growing film.

Ferraria et al. reported a binding energy difference between the C–F component in the F1s spectrum and the C–C component in the C1s spectrum of 402 eV [11]. In our studies we find a difference between the mentioned peaks of 402.0 eV ± 0.2 eV, which is constant for all films, with fluorine contents between 16 at% to 35 at%.

Fig. 5 shows the relative peak area for all assigned contributions as a function of the fluorine content. As expected, the C–C contribution decreases with increasing fluorine content down to 18 at% in the case of 35 at% fluorine in the film. The C1s region for films containing less fluorine, mainly exhibit CF and CF_2 bonds, and, carbon bonds influenced by those components. A minor contribution from CF_3 bonds is also detected. These components show only a slight increase for samples with $x \le 0.23$. As can be further seen in Fig. 5, the slight increase from 23 at% to 26 at% F leads to dramatic changes for all CF_n contributions. Not only the amounts of CF, CF_2, CF_3 bonds increase, but also a new contribution assigned to CF_4 emerges. From this point on, C1s spectra are dominated by signals originating from carbon that has reacted with fluorine. We note that there is a correlation between the sudden increase in the amount of CF and CF_2 bonds formed and the observed increase of discharge current. The latter may indicate a rapid increase of charged species in the target vicinity due to a changed secondary electron emission yield of an altered target surface (see discussion on discharge current in Section 3.2). An increase in

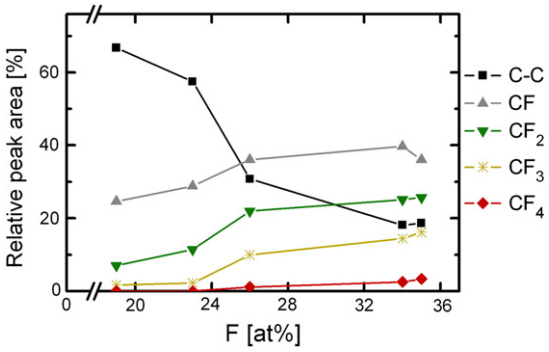

Fig. 5. Relative peak area for the assigned contributions to the C1s peak as a function of the fluorine content.

fluorine content beyond 26 at% further facilitates formation of CF-, CF_2- and CF_3-bonds. The rate of increase in relative contributions from the latter species is similar for samples with $x \leq 0.23$.

Raman spectra of samples with different fluorine contents are presented after background subtraction in Fig. 6. For films with fluorine contents up to 23 at% one broad band (G) with a well developed shoulder (D) is observed. For those films the D-band was located at ~1390 cm^{-1} and the G-band at ~1575 cm^{-1}. Spectra obtained from films containing more than 26 at% fluorine exhibit two well separated bands at ~1390 cm^{-1} (D-band) and ~1610 cm^{-1} (G-band). Thus, increasing fluorine contents yield in a shift of the G-band towards higher frequencies and a decrease in its line width. However, the G-peak is notably well developed and the most prominent feature in all spectra. Both bands appear well separated in spectra of films containing more than 26 at% fluorine. These observations confirm an increasing amount of sp^2 bonds as more fluorine is introduced into the amorphous carbon matrix, which is consistent with our XPS results. It is interesting, that no luminescence was observed for films up to 23 at% fluorine, whereas films with an fluorine content of 26 at% or more showed a high luminescence background. This indicates a graphitic nature of CF_x films with $x \leq 0.23$ and a polymeric structure for films $x \geq 0.26$. Qualitatively, the same trends were observed by Bendavid et al. [8] and Ishihara et al. [9] for CF_x films deposited via PE-CVD and RF-MS, respectively.

The microstructure of the CF_x thin films deposited at low substrate temperature is amorphous based on high resolution TEM images (cf. Fig. 7) in a–c) plan-view and d) cross-section with corresponding SAED patterns for $x = 0.19$, 0.23, 0.26, and 0.35, respectively. No lattice fringes of curved planes could be seen. The SAED patterns, instead, consist of broad diffuse rings (with FWHM of 0.1–0.2 $Å^{-1}$), characteristic for amorphous materials [42]. Specifically, the rings have diameters of ~1.15 Å and ~2.15 Å, which are typical for amorphous carbon allotropes [42]. Moreover, a broad ring of low intensity

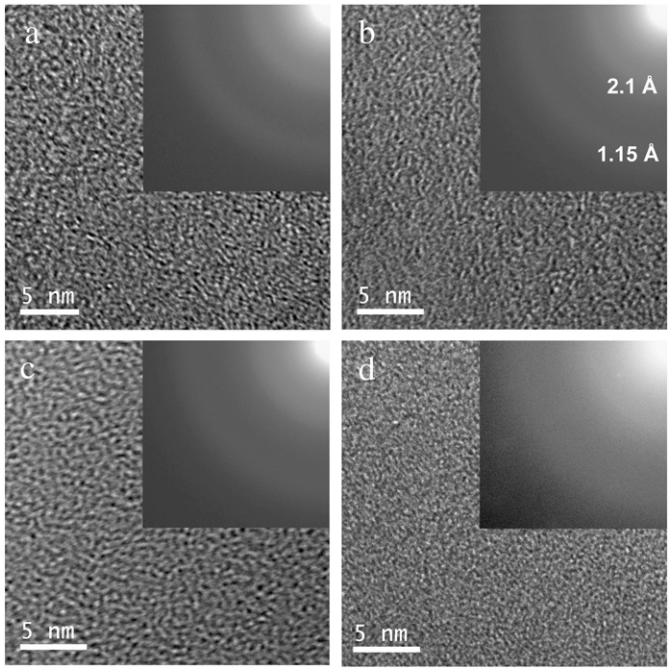

Fig. 7. a–c) Plan-view and d) cross-sectional HR-TEM images with corresponding SAED pattern from CF_x films with $x = 0.19$, $x = 0.23$, $x = 0.26$, $x = 0.35$.

was observed between 0.55 Å and 0.75 Å (not visible in Fig. 7 due to low intensity). The lack of a ring at ~3.5 Å indicates that no graphite or fullerene like short range ordering is present in the films, as was otherwise the case for FL-CN_x thin films [42].

3.4. Effects of fluorine on the mechanical properties of CF_x films

Typical load–displacement curves of four samples with different fluorine contents are shown as inset in Fig. 8. The areas enclosed by load and unload representing indentation induced plastic work, meaning that CF_x posses a very high elasticity, which is comparable to FL-CN_x [3], [33]. This complicates the analysis since an indentation response with hardly any plastic deformation implies a large fraction of elastic deformation and subsequently a region of increased stresses is formed below the indenter. Depending on the film thickness this stressed area might extend into the substrate. For our film thicknesses up to 700 nm and indentation depths of up to 10% of the film thickness, this appears very likely. In the context of maximum indentation depths it is worth mentioning that roughness values (R_q)

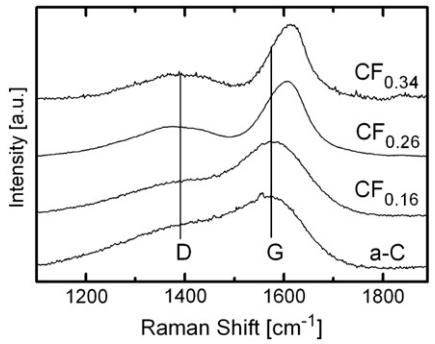

Fig. 6. Raman spectra of CF_x samples with $x = 0$, $x = 0.16$, $x = 0.26$, $x = 0.34$ after background subtraction. D- and G-band positions are indicated at 1390 cm^{-1} and 1575 cm^{-1}, respectively, as obtained from a-C and $CF_{0.16}$.

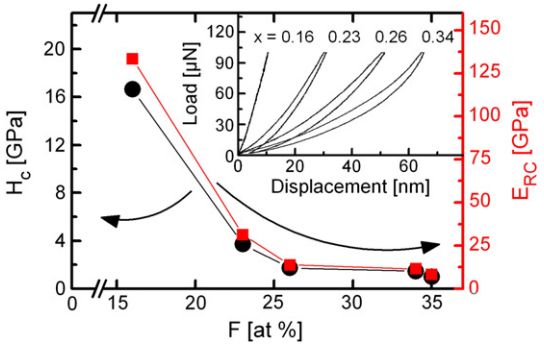

Fig. 8. Composite hardness H_C and reduced composite modulus E_{RC} plotted as a function of the fluorine content of CF_x films. Inset shows typical load–displacement curves of CF_x films with $x = 0.16$, $x = 0.23$, $x = 0.26$ and $x = 0.34$.

for the investigated films ranged between 0.3 nm ± 0.1 nm and 2.1 nm ± 0.1 nm depending on the CF_4 partial pressure; up to 42 mPa R_q was found to increase steadily followed by a decrease for films deposited p_{CF_4}>42 mPa, this mirrors the trend presented for the deposition rate. Considering the elasticity of the films and the indentation depths, it is fair to assume the load–displacement curves reflect a combination of film and substrate response. Consequently, in order to obtain the hardness and reduced modulus of our films, the model suggested by Korsunsky et al. was applied for the analysis [43]. The composite hardness H_C and the reduced composite modulus E_{RC} were thus calculated with the Eqs. (4) and (5):

$$H_C = H_S + \frac{H_F - H_S}{1 + k\beta^2}, \tag{4}$$

$$E_{RC} = E_S + \frac{E_F - E_S}{1 + k\beta^2}, \tag{5}$$

where H_S and E_S are the substrate hardness and modulus, H_F and E_F are the hardness and modulus for the film, respectively. The constant k includes parameters like possible film cracking or delamination from the substrate and is described by the fitting of H_C over β. Eq. (6) is the quotient resulting from the indentation depth δ divided by the film thickness t.

$$\beta = \frac{\delta}{t} \tag{6}$$

Fig. 8 presents the values obtained for the composite hardness H_C and the reduced composite modulus E_{RC} as function of the fluorine content in the films. Increasing fluorine contents result in a decreasing hardness; where H_C for 16 at% fluorine is 16 GPa, and decreases for 35 at% fluorine to a value of ~1 GPa. The reduced modulus follows the same trend; E_{RC} for 16 at% fluorine has a value of 126 GPa, and E_{RC} decreases to 8 GPa for 35 at% fluorine. Furthermore, CF_x shows elastic recoveries decreasing from 98% to 90% in films of fluorine contents ranging between 16 at% and 34 at%. Decreasing values for hardness and elastic modulus with increasing fluorine contents were also found for CF_x films produced via RF-MS and PE-CVD [9], [8]. This behavior can be attributed to a higher degree of polymerization, where larger carbon chains are fractured due to the higher amount of fluorine in the sample, leading to decreased mechanical properties. CF_x films synthesized using HiPIMS show a hardness-to-modulus ratio (H/E ratio) of ~0.12, whereas DLC coatings, classified as elastic material, were found to exhibit an H/E ratio of ~0.1, FL-CN_x, known as super elastic material, ranged between 0.15 and 0.19 [3] and Bendavid et al. indicated H/E ratios of ~0.1 for CF_x films deposited by PE-CVD [8]. Therefore, CF_x films deposited by HiPIMS under the chosen conditions might be considered as highly elastic films.

4. Conclusions

We have demonstrated the synthetic growth of amorphous CF_x thin solid films by HiPIMS deposition and related *ab initio* calculations. The calculations predict that energetically preferred growth precursors are CF, CF_2, C_2 and to a lesser extent free C and F atoms as well as CF_3 radicals.

CF_4 partial pressures below or at 42 mPa produce amorphous films exhibiting a graphitic nature with a fluorine content up to 23 at%. The bonding in these films comprises C–C, CF, CF_2, and very little CF_3. CF_4 partial pressures above 55 mPa lead to an even less ordered polymer-like structure, containing also CF_4 bonding. The maximum fluorine content in the films was 35 at% as obtained for a partial pressure of 80 mPa. For a further addition of CF_4 to the discharge, the structural incorporation of fluorine in the films saturates at 31 at% due to chemical resputtering of volatile C–F species.

The films exhibit a high elasticity and a moderate-to-low hardness compared to diamond-like carbon. Films with fluorine contents of ≤23 at% possess hardnesses between 16 GPa and 4 GPa due to structurally incorporated fluorine in the carbon sheets, giving rise to branching and cross-linking. Higher fluorine contents yield a higher degree of polymerization which softens the films down to ~1 GPa. Furthermore, films with fluorine contents of less than 16 at% could not be grown, due to the highly reactive HiPIMS process.

Acknowledgments

The VINN Excellence Center *Functional Nanoscale Materials (FunMat)* is acknowledged. We are thankful for access to the Tandem Laboratory, Uppsala University. G.K.G. is grateful to the Swedish Research Council. Zsolt Czigány acknowledges the Bolyai Scholarship of the Hungarian Academy of Sciences.

References

[1] N. Hellgren, M.P. Johansson, E. Broitman, L. Hultman, J.-E. Sundgren, Phys. Rev. B 59 (7) (1999) 5162.
[2] A. Furlan, G.K. Gueorguiev, Z. Czigany, H. Hogberg, S. Braun, S. Stafstrom, L. Hultman, Phys. Status Solidi-Rapid Res. Lett. 2 (4) (2008) 191.
[3] J. Neidhardt, L. Hultman, J. Vac. Sci. Technol., A 25 (4) (2007) 633.
[4] E.J. Winder, K.K. Gleason, J. Appl. Polym. Sci. 78 (4) (2000) 842.
[5] S. Agraharam, D.W. Hess, P.A. Kohl, S.A.B. Allen, J. Vac. Sci. Technol., B 19 (2) (2001) 439.
[6] H.S. Jung, H.H. Park, Thin Solid Films 420 (2002) 248.
[7] K. Endo, K. Shinoda, T. Tatsumi, J. Appl. Phys. 86 (5) (1999) 2739.
[8] A. Bendavid, P.J. Martin, L. Randeniya, M.S. Amin, R.R., Diam. Relat. Mater. 19 (2010) 1466.
[9] M. Ishihara, M. Suzuki, T. Watanabe, T. Nakamura, A. Tanaka, Y. Koga, Diam. Relat. Mater. 14 (2005) 989.
[10] C.H. Lai, W.S. Lai, H.C. Chiue, H.J. Chen, S.Y. Chang, S.J. Lin, Thin Solid Films 510 (1–2) (2006) 125.
[11] A.M. Ferraria, J.D.L. da Silva, A.M.B. do Rego, Polymer 44 (23) (2003) 7241.
[12] A. Bendavid, P.J. Martin, L. Randeniya, M.S. Amin, Diamond Relat. Mater. 18 (1) (2009) 66.
[13] C.E. Bottani, A. Lamperti, L. Nobili, P.M. Ossi, Thin Solid Films 433 (1–2) (2003) 149.
[14] L.G. Jacobsohn, D.F. Franceschini, M. da Costa, F.L. Freire, J. Vac. Sci. Technol., A 18 (5) (2000) 2230.
[15] M. Samuelsson, D. Lundin, J. Jensen, M.A. Raadu, J.T. Gudmundsson, U. Helmersson, Surf. Coat. Technol. 205 (2) (2010) 591.
[16] Y. Lifshitz, S.R. Kasi, J.W. Rabalais, W. Eckstein, Phys. Rev. B 41 (15) (1990) 10468.
[17] J. Weichart, M. Elghazzali, S. Kadlec, A.P. Ehiasarian, Proceeding of the 52nd Annual Technical Conference of the Society of Vacuum Coaters, May 9–14, 2009, Santa Clara, CA, USA, 2009, p. 201.
[18] B.M. DeKoven, P.R. Ward, R.E. Weiss, D.J. Christie, R.A. Scholl, W.D. Sproul, F. Tomasel, A. Anders, in: S.o.V. Coaters (Ed.), 46th Annual Technical Conference San Francisco, CA, USA, 2003, p. 158.
[19] V. Kouznetsov, K. Macak, J.M. Schneider, U. Helmersson, I. Petrov, Surf. Coat. Technol. 122 (2–3) (1999) 290.
[20] W.-D. Münz, M. Schenkel, S. Kunkel, J. Paulitsch, K. Bewilogua, J. Phys. Conf. Ser. 100 (8) (2008).
[21] G.K. Gueorguiev, E. Broitman, A. Furlan, S. Stafstrom, L. Hultman, Chem. Phys. Lett. 482 (1–3) (2009) 110.
[22] M.J. Frisch, Gaussian 03, Revision C.02, Gaussian Inc, Wallingford, CT, 2004.
[23] J.P. Perdew, J.A. Chevary, S.H. Vosko, K.A. Jackson, M.R. Pederson, D.J. Singh, C. Fiolhais, Phys. Rev. B: 46 (11) (1992) 6671.
[24] R.H. Xie, G.W. Bryant, L. Jensen, J.J. Zhao, V.H. Smith, J. Chem. Phys. 118 (19) (2003) 8621.
[25] http://www.cemecon.de/coating_technology/2_coating_units/22_cc_800sup_sup_9_ml/index_eng.htmlJune 2011.
[26] H.J. Whitlow, G. Possnert, C.S. Petersson, Nucl. Instrum. Methods Phys. Res., Sect. B: Beam Interact. Mater. Atoms 27 (3) (1987) 448.
[27] J. Jensen, D. Martin, A. Surpi, T. Kubart, Nucl. Instrum. Methods Phys. Res., Sect. B: Beam Interact. Mater. Atoms 268 (11–12) (1893).
[28] J.L. Labar, Microsc. Microanal. 15 (1) (2009) 20.
[29] W. Schwarzenbach, A. Tserepi, J. Derouard, N. Sadeghi, Jpn. J. Appl. Phys. Part 1 — Regul. Pap. Short Notes Rev. Pap. 36 (7B) (1997) 4644.
[30] G.K. Gueorguiev, J. Neidhardt, S. Stafstrom, L. Hultman, Chem. Phys. Lett. 410 (4–6) (2005) 228.
[31] G.K. Gueorguiev, A. Furlan, H. Hogberg, S. Stafstrom, L. Hultman, Chem. Phys. Lett. 426 (4–6) (2006) 374.
[32] C.P., 91st ed., CRC Handbook of Chemistry and Physics, 2010.
[33] J. Neidhardt, L. Hultman, B. Abendroth, R. Gago, W. Moller, J. Appl. Phys. 94 (11) (2003) 7059.
[34] K. Sarakinos, J. Alami, S. Konstantinidis, Surf. Coat. Technol. 204 (11) (2010) 1661.
[35] B.K. Antony, K.N. Joshipura, N.J. Mason, J. Phys. B: At. Mol. Opt. Phys. 38 (3) (2005) 189.
[36] G. Greczynski, L. Hultman, Vacuum 84 (9) (2010) 1159.

[37] M. da Costa, F.L. Freire, L.G. Jacobsohn, D. Franceschini, G. Mariotto, I.R.J. Baumvol, Diamond Relat. Mater. 10 (3–7) (2001) 910.
[38] Y.G. Lei, K.M. Ng, L.T. Weng, C.M. Chan, L. Li, Surf. Interface Anal. 35 (10) (2003) 852.
[39] C. Ronning, M. Buttner, U. Vetter, H. Feldermann, O. Wondratschek, H. Hofsass, W. Brunner, F.C.K. Au, Q. Li, S.T. Lee, J. Appl. Phys. 90 (8) (2001) 4237.
[40] J.P. Chang, H.W. Krautter, W. Zhu, R.L. Opila, C.S. Pai, J. Vac. Sci. Technol., A 17 (5) (1999) 2969.
[41] H.N. Yang, D.J. Tweet, Y.J. Ma, T. Nguyen, Appl. Phys. Lett. 73 (11) (1998) 1514.
[42] Z. Czigany, L. Hultman, Ultramicroscopy 110 (7) (2010) 815.
[43] A.M. Korsunsky, M.R. McGurk, S.J. Bull, T.F. Page, Surf. Coat. Technol. 99 (1–2) (1998) 171.